Viscoelastic convection: Few-modes model and numerical simulations of field equations for Maxwellian fluids

M. Salm* and M. Lücke
Institut für Theoretische Physik, Universität des Saarlandes, D-66123 Saarbrücken, Germany
(Received 17 October 2011; revised manuscript received 25 July 2012; published 15 October 2012)

The structure formation of convection rolls in Maxwellian fluids that are heated from below in a Rayleigh-Bénard setup is investigated close to onset with a simple few-modes ansatz and by solving the hydrodynamic field equations with a finite-difference method. Depending on the magnitude of the viscoelastic relaxation time one can have besides stationary convection also oscillatory patterns in the form of standing or traveling waves. The existence and stability regions of these convection structures are determined. The convection behavior of the model is compared with the results of full numerical simulations. Furthermore, the effect of modulating the heating periodically in time on the stability of the quiescent conductive state of the fluid and on its convection behavior is investigated as a function of the fluid's viscoelasticity.

DOI: 10.1103/PhysRevE.86.046312 PACS number(s): 47.20.Ky, 47.11.Bc, 47.20.Gv

I. INTRODUCTION

The Rayleigh-Bénard system [1,2] is a well-known hydrodynamic setup which provides an easy experimental and theoretical access to a very rich variety of flow structures [3]. When the temperature difference between the two horizontal plates exceeds a critical threshold, convection rolls and further flow patterns arise. With binary mixtures as working fluid, the so-called Soret coupling between temperature differences and concentration fluxes [4] leads to a new type of instability at the critical threshold: the system responds oscillatorily [5]. During recent decades, another class of fluids, namely, the viscoelastic fluids, has been investigated intensively [6] because of the presence of intrinsic elastic restoring forces. This circumstance and the existence of the associated additional degrees of freedom can also cause overstability [7] and oscillatory convection.

We study here the convection of Maxwellian fluids in the Oberbeck-Boussinesq approximation [4] in order to concentrate on the essential parts of the problem that causes oscillatory behavior in the form of traveling and standing convection waves. The relevant system parameters are the Rayleigh number Ra, the Prandtl number Pr, and the Deborah number De, which is proportional to the viscoelastic time scale λ. The value of De strongly affects the flow behavior. Below a certain value $\mathrm{De} \lesssim \mathrm{De}^*$, the fluid shows the characteristics of a Newtonian fluid [7], for instance a stationary instability. Above the critical value $\mathrm{De} \gtrsim \mathrm{De}^*$, the fluid shows an oscillatory instability. We investigate this behavior in two dimensions by using the Galerkin and finite-difference methods [8]. While these methods have been tested intensively for a lot of fluids and systems, they are restricted to small Deborah and Rayleigh numbers due to numerical instabilities [9].

The Lorenz model [10] allows an alternative insight into the instability mechanisms of a Newtonian fluid without the efforts that are connected to full numerical simulations. We study in this paper among others a kind of enlarged and generalized model with three complex field modes and one real mode. It is capable of describing viscoelastic effects of convecting Maxwellian fluids including traveling waves and standing waves on a very basic level. On the other hand, if one takes into account only real field amplitudes then one loses the oscillatory instability that shows up in the Maxwell approach above a certain Deborah number De^* since the restricted mode ansatz allows only roll structures that are stationary close to onset and that show only at higher Rayleigh numbers the transition from oscillatory to chaotic amplitude behavior known from the standard Lorenz model [11]. This type of analysis was expanded to other fluids such as the Carreau-Bird fluid [12] and the Oldroyd-B fluid [13]. Recently the effect of time-periodic gravity modulation on convection rolls in Oldroyd-B fluids was investigated with a few-modes truncation that is similar to ours [14].

Several authors have addressed the linear problem associated with the onset of convection in different types of fluid model equations starting with the early work of Vest and Arpaci [7] and Sokolov and Tanner [15]. Later on Eltayeb [16] and Martínez-Mardones and Pérez-García [17] published a similar analysis for the Oldroyd-B fluid. All these results predict an oscillatory instability depending on the viscoelastic time scale. Rosenblat [18] and Park and Lee [19] used a model that can be projected on either an Oldroyd-B or a Phan-Thien-Tanner model. They analyzed the subcritical and supercritical behavior of periodic solutions and they investigated traveling and standing wave convection structures at onset. Brand and Zielinska [20] and Zielinska *et al.* [21] derived nonlinear amplitude equations around the codimension-2 point of a linear Maxwell fluid with an advective term in the constitutive equations. Martínez-Mardones et al. [22–24] also discussed amplitude equations for Jeffreys fluids. They found that the flow structure and the bifurcation properties strongly depend on the chosen constitutive equations. Based on Ginzburg-Landau amplitude equations, they predicted that for a wide range of parameters the stable solution of an Oldroyd-B model is a supercritical standing wave solution and that subcritical bifurcations and polycritical points will occur only under unrealistic conditions if one includes the upper-convected time derivative.

Our paper is organized as follows. In Sec. II we present the governing equations and the few-modes model. Section III is

*m.salm@lusi.uni-sb.de

devoted to linear as well as nonlinear aspects of the bifurcation to stationary roll convection, traveling waves, and standing waves. The latter were analyzed not only with the few-modes model but also with numerical finite-difference simulations of the linear Maxwell fluid (LFM) and the upper convected Maxwell fluid (UCM). In Sec. IV, we present results for time-modulated heating that were obtained from our few-modes model and from finite-difference simulations.

II. SYSTEM

Let us consider two horizontal plates with a distance d between them, that are perpendicular to the external gravitational field $\mathbf{g}$ and that are kept at temperatures T_1 (lower) and T_2 (upper). They enclose a viscoelastic fluid, that is described by a viscoelastic relaxation time λ [25]. The coefficients of volumetric expansion, thermal conductivity, and kinematic viscosity are denoted by α, κ, and ν, respectively.

A. Basic field equations

We neglect the elastic energy and obtain within the Oberbeck-Boussinesq approximation the dimensionless basic equations

$$0 = \nabla_i u_i, \tag{2.1a}$$

$$(\partial_t + \mathbf{u}\cdot\boldsymbol{\nabla})u_i = -\nabla_i \mathcal{P} + \mathrm{Pr}\,\nabla_j \mathcal{T}_{ji} + \mathrm{Pr}\,\theta\delta_{i3}, \tag{2.1b}$$

$$(\partial_t + \mathbf{u}\cdot\boldsymbol{\nabla})\ \theta = \mathrm{Ra}\,w + \nabla^2\theta \tag{2.1c}$$

for the velocity field $\mathbf{u} = (u,v,w)$, the hydrostatic pressure $\mathcal{P}$, and the perturbations of the conductive temperature profile $\theta = T - T_{\mathrm{cond}}$. To transform them to a dimensionless form, we used the system height d as length scale, the thermal diffusion time d^2/κ as time scale, and, consequently, κ/d as velocity scale. The dimensionless quantities lead to new system parameters, namely, the Rayleigh number

$$\mathrm{Ra} = \frac{\alpha g d^3}{\nu\kappa} \tag{2.1d}$$

measuring the thermal driving force and the Prandtl number

$$\mathrm{Pr} = \frac{\nu}{\kappa} \tag{2.1e}$$

as the ratio of the thermal diffusion time to the momentum diffusion time. The Prandtl number is fixed here throughout this paper to $\mathrm{Pr} = 10$.

The constitutive equations of an upper-convected Maxwell fluid can, by the help of the shear rate $\dot\gamma_{ij} = \nabla_i u_j + \nabla_j u_i$, be expressed [11,25] by

$$(\partial_t + \mathbf{u}\cdot\boldsymbol{\nabla})\mathcal{T}_{ij} = \mathcal{T}_{kj}\nabla_k u_i + \mathcal{T}_{ik}\nabla_k u_j + \frac{1}{\mathrm{De}}(\dot\gamma_{ij} - \mathcal{T}_{ij}), \tag{2.1f}$$

where $\mathcal{T}_{ij} = \mathcal{T}_{ji}$ [26] represents the stress tensor. The Deborah number

$$\mathrm{De} = \lambda\frac{\kappa}{d^2} \tag{2.1g}$$

is the viscoelastic relaxation time λ measured in units of the thermal diffusion time. It characterizes the elastic properties of the fluid. The Newtonian case is realized within the limit $\mathrm{De}\to 0$.

The boundary conditions of the velocity field mainly influence the absolute values of the critical thresholds. This influence can be minimized by the use of reduced parameters; we discuss this further below. Furthermore, the boundary conditions have an impact on the critical fields and, thus, on the ansatz functions. In order to simplify the model as far as possible, we choose free-slip conditions at both plates, which allows us to expand the velocity fields by simple trigonometric functions [7]. We also checked that numerical results for no-slip boundary conditions showed qualitatively the same behavior.

We implemented a finite-difference method based on the work of Hirt *et al.* [27] and Harlow and Welch [28]. Additionally, this simulation contains the discretized constitutive equations of the stress tensor.

B. Model

The derivation of the model equations largely follows the work of Khayat [11]. Therefore we summarize here only the most important steps in our derivation.

Our aim is a Lorenz-like system for weakly viscoelastic, Maxwellian fluids. A suitable approach consists of keeping the critical modes as well as one nonlinear field mode which generates the vertical heat current [10]. Then, all coupling terms in the constitutive equations vanish. Furthermore, the differences between the upper-convected and the linear Maxwell fluid vanish with this choice of ansatz functions. Finally, it is sufficient to take within this approximation only the divergence of the stress tensor into consideration. In this way we find a new representation of the stress field as

$$\mathcal{S} = \left(\partial_x^2 - \partial_z^2\right)\mathcal{T}_{xz} + \partial_x\partial_z(\mathcal{T}_{zz} - \mathcal{T}_{xx}). \tag{2.2}$$

Consequently, the resulting few-modes approximation is

$$\Upsilon(x,z,t) = [\hat\Upsilon_{11}(t)e^{ikx} + \mathrm{c.c.}]\sqrt{2}\sin\pi z, \tag{2.3a}$$

$$\mathcal{S}(x,z,t) = [\hat{\mathcal{S}}_{11}(t)e^{ikx} + \mathrm{c.c.}]\sqrt{2}\sin\pi z, \tag{2.3b}$$

$$\theta(x,z,t) = [\hat\theta_{11}(t)e^{ikx} + \mathrm{c.c.}]\sqrt{2}\sin\pi z + \hat\theta_{02}(t)\sqrt{2}\sin 2\pi z. \tag{2.3c}$$

Here Υ is the stream function with

$$\partial_x\Upsilon = w \quad\text{and}\quad \partial_z\Upsilon = -u \tag{2.4}$$

so that the mass balance equation (2.1a) is automatically fulfilled. After projection on the orthonormal ansatz functions, we obtain the model equations

$$\tau\partial_t\begin{pmatrix} W\\ X\\ Y\\ Z\end{pmatrix} = \begin{pmatrix} -\delta & -\delta & 0 & 0\\ \mathrm{Pr} & 0 & \mathrm{Pr} & 0\\ 0 & r & -1 & 0\\ 0 & 0 & 0 & -\beta\end{pmatrix}\begin{pmatrix} W\\ X\\ Y\\ Z\end{pmatrix} + \begin{pmatrix} 0\\ 0\\ -XZ\\ \mathrm{Re}(YX^*)\end{pmatrix}. \tag{2.5}$$

The critical mode amplitudes

$$X = \frac{2\pi k}{Q^2}\hat\Upsilon_{11}, \quad Y = -i\frac{2\pi k^2}{Q^6}\hat\theta_{11}, \quad\text{and}\quad W = \frac{2\pi k}{Q^6}\hat{\mathcal{S}}_{11} \tag{2.6}$$

usually are complex. In (2.5) X^* denotes the complex conjugate of X. On the other hand, the amplitude of the nonlinear mode

$$Z = -\frac{\sqrt{2}\pi k^2}{Q^6}\hat{\theta}_{02} \tag{2.7}$$

has to be real. Here, $Q^2 = \pi^2 + k^2$. All amplitudes depend on time t and on the wave number k of the roll pattern. Also the parameters entering the model besides the Prandtl number depend on k. They are

$$r = \frac{\mathrm{Ra}}{\mathrm{Ra}_{\mathrm{stat}}}, \quad \tau = \frac{1}{Q^2}, \quad \delta = \frac{\tau}{\mathrm{De}}, \quad \beta = 4\pi^2\tau. \tag{2.8}$$

Here r is the Rayleigh number Ra (2.1d) normalized by the stationary stability threshold,

$$\mathrm{Ra}_{\mathrm{stat}}(k) = \frac{Q^6}{k^2}. \tag{2.9}$$

The characteristic time scale τ of the model could be eliminated by reducing the time t further, but we will not do that here. Finally, along with the inverse of the Deborah number the viscoelastic relaxation rate enters into δ. The Newtonian limit $\mathrm{De} \to 0$, i.e., $\delta \to \infty$, leads to the well-known standard Lorenz model with $W = -X$.

As an aside we mention that the model system (2.5) can be transformed to a single differential equation of third order:

$$\begin{aligned} 0 = {} & \dddot{X} + \frac{\delta+1}{\tau}\ddot{X} + \left[\frac{\mathrm{Pr}+1}{\tau^2}\delta - \frac{\mathrm{Pr}}{\tau^2}(r - Z[X])\right]\dot{X} \\ & + \frac{\mathrm{Pr}}{\tau^2}\left[\frac{\delta}{\tau} - \dot{r} + \frac{\beta}{\tau}Z[X] - \frac{\delta}{\tau}(r - Z[X])\right. \\ & \left. + \frac{1}{2\,\mathrm{Pr}}(X\dot{X}^* - XW^*[X] + \mathrm{c.c.})\right]X, \end{aligned} \tag{2.10}$$

into which enter, however, two memory functions,

$$W[X] = -\frac{\delta}{\tau}\int_0^\infty X(t-t')e^{-(\delta/\tau)t'}\,dt', \tag{2.11a}$$

$$\begin{aligned} Z[X] = {} & \frac{\tau}{2\mathrm{Pr}}\int_0^\infty [X(t-t')\dot{X}^*(t-t') \\ & - X(t-t')W^*(t-t') + \mathrm{c.c.}]e^{-(\beta/\tau)t'}\,dt'. \end{aligned} \tag{2.11b}$$

III. STATIONARY DRIVING

The case of a stationary driving, i.e., $\Delta T = T_1 - T_2 = \mathrm{const}$ was already considered by Khayat [11], but with the restriction to real field amplitudes in Eq. (2.5). This restriction allows only roll structures that are stationary close to onset and that show at higher Rayleigh numbers the chaotic amplitude behavior known from the standard Lorenz model. But, as mentioned before, in reality the elastic forces support an oscillatory instability that shows up in the Maxwell approach above a certain Deborah number De^*. After having summarized the relevant linear results we discuss in this section the two nonlinear oscillatory solutions of our model, namely the traveling wave (TW) and the standing wave (SW) solutions and also the stability exchange between them.

A. Linear results

Within the Maxwell model the linear theory predicts the stationary thresholds to be independent of the Deborah number while the oscillatory thresholds depend on De [7,15,16,18]. In our few-modes model, one finds first of all that the dominant eigenvalue is real for $\delta > \delta^* = \frac{\mathrm{Pr}}{\mathrm{Pr}+1}$. And then a family of stable solutions describing so-called stationary overturning convection (SOC) with wave number k bifurcates at $r = 1$, i.e., at $\mathrm{Ra} = \mathrm{Ra}_{\mathrm{stat}}(k)$ forwards out of the quiescent conductive state. Furthermore, the squared flow amplitude grows linearly with the distance from the respective threshold since $X^2 = \beta(r-1)$ and $W = -X = -Y$ [11].

For smaller values of δ, overstability can be found. But the oscillatory threshold curve

$$r_{\mathrm{osc}} = \frac{\mathrm{Ra}_{\mathrm{osc}}(k)}{\mathrm{Ra}_{\mathrm{stat}}(k)} \tag{3.1}$$

is restricted to lie below the stationary onset, i.e., $r_{\mathrm{osc}} < 1$. The corresponding Hopf frequency ω_H is a function of the reduced inverse Deborah number δ and the Prandtl number Pr:

$$r_{\mathrm{osc}} = \frac{\delta}{\mathrm{Pr}}[\delta(\mathrm{Pr}+1)+1], \tag{3.2a}$$

$$\omega_H^2\tau^2 = \mathrm{Pr}\,\delta(1-\delta) - \delta^2. \tag{3.2b}$$

Note that r_{osc} and ω_H in eqs. (3.2) depend on the wave number k via the parameters δ and τ.

The linear equation leading to this result (3.2) consists of four terms:

$$\begin{aligned} 0 = {} & \mathrm{De}\dddot{X} + \left(1 + \frac{\mathrm{De}}{\tau}\right)\ddot{X} \\ & + \left(\frac{\mathrm{Pr}+1}{\tau} - \frac{\mathrm{Pr}\,r\,\mathrm{De}}{\tau^2}\right)\dot{X} + \frac{\mathrm{Pr}(1-r)}{\tau^2}X, \end{aligned} \tag{3.3}$$

where the term proportional to $\dot{X}$ is mainly responsible for the oscillatory instability and the one proportional to X generates the stationary instability. Interestingly enough, the first term $\mathrm{De}\dddot{X}$ does not have a big impact on the linear eigenvalues close to the transition point δ^* and $r \sim 1$.

B. Traveling wave solution

In a relaxed TW the fields do not depend on x and t separately since they move with the constant phase velocity $v_{\mathrm{ph}} = \omega_{\mathrm{TW}}/k$ either to the right or to the left. Thus, the moduli of the complex field amplitudes X, Y, and W are constant in time while their phases increase linearly in t.

The TW solution branch can easily be found for $\delta(\mathrm{Pr}+1)+1 > 0$ to vary as

$$|X|^2 = s_{\mathrm{TW}}\mu \tag{3.4a}$$

where

$$s_{\mathrm{TW}} = \beta(1-\delta) \tag{3.4b}$$

denotes the (initial) slope of the squared modulus $|X|^2$ in a bifurcation diagram and

$$\mu = \frac{r}{r_{\mathrm{osc}}} - 1 \tag{3.5}$$

is the relative distance to the oscillatory bifurcation threshold (3.2a).

The TW solution always bifurcates forward out of the basic state [24] since the oscillatory instability occurs only for $\delta < \mathrm{Pr}/(\mathrm{Pr}+1) < 1$. Due to the simplicity of the model equation, the TW frequency does not vary with the Rayleigh number r. The TW frequency is always equal to the corresponding Hopf frequency (3.2b),

$$\omega_{\mathrm{TW}} = \omega_H. \tag{3.6}$$

C. Standing wave solution

In a SW the fields oscillate in time while their nodes remain spatially fixed. In contrast to the TW case we could not obtain a closed analytical solution for, say, the complex mode amplitude $X(t;\mu)$ as a function of time and control parameter μ. So we performed an expansion in powers of $\mu^{1/2}$ around the oscillatory onset $\mu = 0$.

One finds the complex SW mode amplitude $X_{SW}(t;\mu)$ to have in lowest order $\mu^{1/2}$ the harmonic form

$$X_{\mathrm{SW}}(t;\mu) = |X_1| e^{i\omega_{\mathrm{SW}} t} + \mathrm{c.c.} \tag{3.7}$$

with

$$|X_1|^2 = s_{\mathrm{SW}}\mu, \tag{3.8a}$$

$$\omega_{\mathrm{SW}} = \omega_H + \alpha_{\mathrm{SW}}\mu. \tag{3.8b}$$

Here ω_H is the Hopf frequency of the SW at onset. From a solvability condition in order $\mu^{3/2}$ one then obtains the initial slopes of the variation of $|X|^2$ and of ω_{SW} with μ to read

$$s_{\mathrm{SW}} = r_{\mathrm{osc}} \frac{\mathrm{Pr}(1-\delta)}{\delta} \frac{1 - \frac{(\beta+2)q_{\mathrm{osc}}^2}{\Lambda_{\mathrm{osc}}}\left(\mathrm{Pr} + \frac{1}{1-\delta}\right)}{\frac{2}{\beta} + \frac{\beta - 2\omega_H^2\tau^2}{\gamma_{\mathrm{osc}}^2}}, \tag{3.9a}$$

$$\alpha_{\mathrm{SW}} = -r_{\mathrm{osc}} \frac{(\beta+2)\mathrm{Pr}^2 q_{\mathrm{osc}}^2}{2\omega_H^2\tau^2\Lambda_{\mathrm{osc}}}, \tag{3.9b}$$

using the abbreviations

$$q_{\mathrm{osc}}^2 = \delta^2 + \omega_H^2\tau^2, \tag{3.10a}$$

$$\gamma_{\mathrm{osc}}^2 = \beta^2 + 4\omega_H^2\tau^2, \tag{3.10b}$$

$$\Lambda_{\mathrm{osc}} = (\beta+2)\left(\mathrm{Pr} + \frac{1}{1-\delta}\right) q_{\mathrm{osc}}^2 - \left(\frac{2}{\beta}\gamma_{\mathrm{osc}}^2 + \beta - 2\omega_H^2\tau^2\right)\mathrm{Pr}. \tag{3.10c}$$

The term Λ_{osc} in Eq. (3.9b) causes the divergence of the initial slope at the tricritical transition from forward to backward bifurcation. It is straightforward to obtain the quadratic equation

$$\delta^2\left[2\frac{\mathrm{Pr}+1}{\mathrm{Pr}}\frac{4-\beta}{\beta} - (\beta+2)\right] + \delta\left[2\frac{\beta-4}{\beta} + (\beta+2)\frac{\mathrm{Pr}+1}{\mathrm{Pr}}\right] = \frac{3\beta}{\mathrm{Pr}} \tag{3.11}$$

for the condition $\Lambda_{\mathrm{osc}} = 0$ for the occurrence of the tricritical SW transition. The phase diagram in Fig. 1 shows the parameter regions in the k-De plane for forward and backward SW bifurcations, respectively. Note the small interval of forward SW bifurcation adjacent to the stationary regime. Thus, there are in the k-De plane two lines locating tricritical SW transitions. These tricritical lines delimit in Fig. 1 the region marked "Backward" for backward bifurcating SWs.

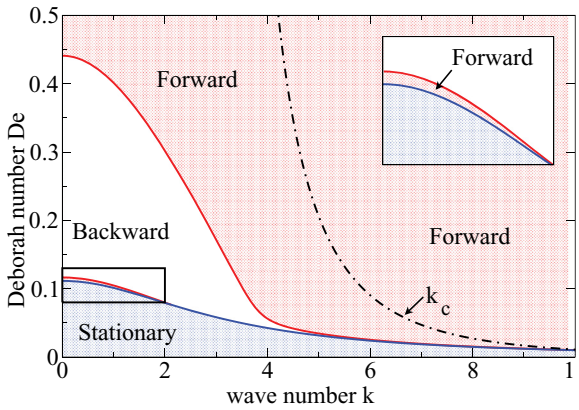

FIG. 1. (Color online) Phase diagram in the k-De plane for forward and for backward bifurcating SW convection, respectively, and for stationary convection. The critical relation between wave number and Deborah number is shown by the dash-dotted line labeled k_c.

Furthermore, backward bifurcating SWs occur only with small wave numbers when the Deborah number is not too big. However, it is hard to stabilize SW roll patterns with small wave numbers $k \ll k_c$ in numerical simulations and presumably also in real experiments. Our numerical finite-difference simulations support this conclusion. All SW patterns that we observed bifurcated forward.

Figure 2 presents the results of numerical integrations of the few-modes model (2.5) and of numerical finite-difference simulations of both the linear Maxwell model (circles) and the upper-convected Maxwell model (squares). The SW Nusselt number Nu as a ratio between the total heat flux and the conductive heat flux oscillates in time. Thus, we indicated its minimum and maximum over the period $2\pi/\omega_{\mathrm{SW}}$. The Nusselt numbers of the few-modes model and of the linear Maxwell model are—in particular close to the onset of SW convection—in good agreement with the results of the upper-convected Maxwell model. The SW frequencies of the linear models increase only very weakly with increasing Rayleigh numbers. On the other hand, the nonlinearities in the constitutive equations of the upper-convected Maxwell model seem to be responsible for the stronger growth of the SW frequencies with increasing r.

D. Stability

Close to the oscillatory threshold perturbation theory leading to coupled amplitude equations allows one to determine the stability of extended TWs and SWs [29,30]. The stability depends on the initial slope with which the squared TW and SW amplitudes grow with increasing distance from the common Hopf bifurcation threshold. The result is that the structure with the smaller initial slope is unstable and dies out.

The result of such a stability analysis of our few-modes model is shown in the k-De parameter plane of Fig. 3 for TWs and SWs with wave numbers $2 \leqslant k \leqslant 8$. Note first of all that

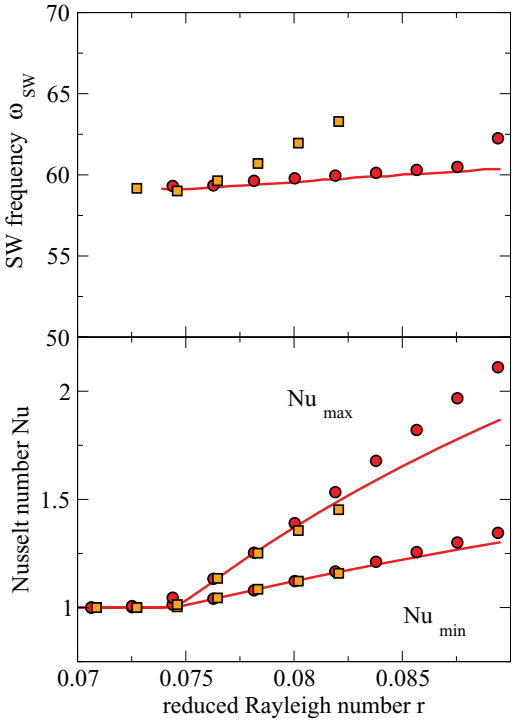

FIG. 2. (Color online) Nusselt number (lower figure) and frequency (upper figure) of SW solutions of different approaches versus reduced Rayleigh number r: Finite-difference simulations of the linear Maxwell fluid (circles), finite-difference simulations of the upper-convected Maxwell model (squares), and truncated model (2.5) (full lines). For the Nusselt number the minimum $\mathrm{Nu}_{\mathrm{min}} = \min_t \mathrm{Nu}(t)$ and the maximum $\mathrm{Nu}_{\mathrm{max}} = \max_t \mathrm{Nu}(t)$ are shown. The parameters are $k = 6$ and $\mathrm{De} = 0.1$.

the model allows stable, forward bifurcating TW solutions. However, they occur at quite large Deborah numbers that are well beyond the range of applicability of this simple model. The transient times from the disturbed conductive basic state to the final stable TWs are quite large even for large thermal driving $\mu > 0.05$.

E. Deborah number

At higher Deborah numbers, the oscillatory threshold flattens and the corresponding critical Rayleigh number decreases. Consequently, a larger interval of unstable wave numbers exists close to onset.

Moreover, numerical instabilities occur [8,31]. Several authors have addressed the numerical instabilities and discussed them [32–34]. In our simulations at higher elasticity, the results of the numerical simulations begin to depend on numerical parameters. At even higher values of De, the pressure iteration fails.

If we use the rate of advection as the time scale for the definition of the Deborah number $\mathrm{De}_{\mathrm{shear}} = \lambda \frac{\tilde{w}_{\mathrm{max}}}{d}$ then its values may change considerably since the convection amplitude $\tilde{w}_{\mathrm{max}}$ enters and is not reduced here. The difference can be expressed by the Péclet number as follows:

$$\frac{\mathrm{De}_{\mathrm{shear}}}{\mathrm{De}} = \mathrm{Pe} = w_{\mathrm{max}}. \tag{3.12}$$

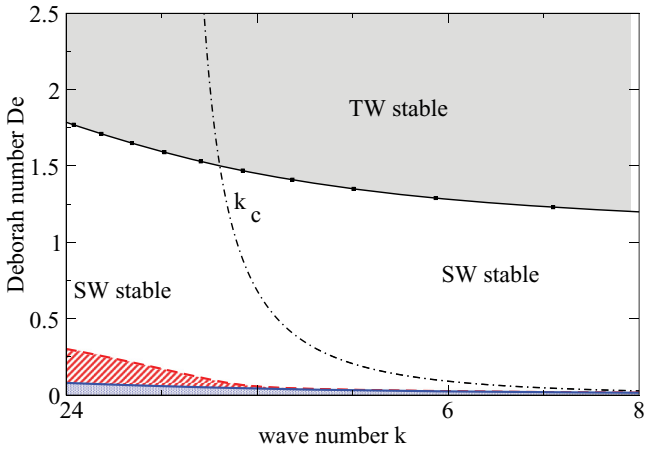

FIG. 3. (Color online) Stability behavior of forward bifurcating TWs and SWs of the few-modes model close to the Hopf bifurcation threshold obtained from a perturbation analysis. The regime with stationary convection (close to the abscissa) and the one with backward bifurcating SWs (stripes) are included for the sake of completeness. The narrow interval of forward bifurcating SWs close to the stationary regime that can be seen in Fig. 1 is not resolved here. The dash-dotted line marks the critical wave number k_c.

For example, for a SW structure of $\mu = 0.05$, $\mathrm{De} = 0.1$, and $k = 5$, the resulting Péclet number is around 10 and, thus, $\mathrm{De}_{\mathrm{shear}} \sim 1$.

IV. MODULATED DRIVING

In the previous section we investigated the oscillatory convection that arises in viscoelastic fluids because of the elastic restoring forces. In this section we explore how this system, which shows under stationary driving oscillations with the internal characteristic TW or SW frequency, ω_{TW} or ω_{SW}, respectively, responds to external imposition of an oscillation of the thermal driving force. For the sake of simplicity we consider only a harmonic modulation of the temperature difference between the lower and the upper plates,

$$\Delta T(t) = \Delta T_{\mathrm{stat}} + \Delta T_{\mathrm{mod}}(t) = \mathrm{Ra}[1 + \Delta \cos \Omega t]. \tag{4.1}$$

Here Δ is the relative modulation amplitude and $\mathrm{Ra}(t) = \mathrm{Ra}[1 + \Delta \cos \Omega t]$ is the instantaneous Rayleigh number.

In the presence of such a modulation of the thermal driving the vertical variation of the temperature field in the quiescent conductive basic state, $T_{\mathrm{cond}}(z,t)$, is no longer linear in z but becomes nonlinear. However, the analytical expression for $T_{\mathrm{cond}}(z,t)$ is obtained straightforwardly by solving the heat diffusion equation.

We performed a linear Floquet stability analysis of this conductive state using a many-mode Galerkin expansion for a linear Maxwell fluid and we compared that with the result of our modulated few-modes model; cf. Sec. III A. Then we present in Sec. IV C for small Deborah numbers the results of full, nonlinear numerical simulations for a linear Maxwell fluid and for an upper-convected Maxwell fluid.

A. Modulated few-modes model

Here we want to mention that the temperature modulation (4.1) does not change the structure of the few-modes model (2.5). However, the stationary reduced Rayleigh number r in (2.5) is replaced by the time-dependent quantity

$$\tilde{r}(t) = r\mathrm{Re}[1 + \tilde{\Delta}e^{i\Omega t}]. \tag{4.2}$$

The complex modification $\tilde{\Delta}$ of the modulation amplitude of the plate's temperature difference enters into the model via the $\sin(2\pi z)$ contribution to the conductive profile $T_{\mathrm{cond}}(z,t)$ [35]. On has

$$\tilde{\Delta} = \Delta\frac{4\pi^2}{4\pi^2 + i\Omega}. \tag{4.3}$$

The modulus $|\tilde{\Delta}|$ of the correction approaches Δ for small frequencies and vanishes for very large modulation frequencies.

B. Linear stability analysis

We integrated the fundamental matrix of the linearized, modulated few-modes model over one modulation period $\underline{\Phi}(t_0 + T) = \underline{\Phi}(t_0)\cdot\underline{E}$ and obtained the Floquet multipliers $\mu = \exp(\rho T)$ from the eigenvalues of $\underline{E}$ [36,37]. We have chosen $\underline{\Phi}(t_0)$ to be the 6×6 unit matrix that contains in its columns the six orthogonal initial values for the vector (W,X,Y) with W,X,Y being complex—the real mode Z is decoupled and damped away within the linearized few-modes model. Then $\underline{E} = \underline{\Phi}(t_0 + T)$ is obtained from numerical integration over one modulation period.

The real parts of the Floquet exponents ρ describe the stability of the modulated conductive solution against growth of convective perturbations, whereas the imaginary parts describe the phase shift of the solution after one modulation period. The stability threshold is determined by the condition that the largest real part goes through zero.

We performed the same calculation for linearized multimode Galerkin models and calculated for both scenarios the stability thresholds for free-slip boundary conditions. Unlike the results obtained in the unmodulated case, the linear stability results obtained with a many-mode Galerkin expansion from the linearized field equations differ slightly from those of the few-modes model. The reason is that the mode truncation represents the conductive temperature profile $T_{\mathrm{cond}}(z,t)$ and the convective perturbation fields only approximately. However, we checked that for modulation frequencies $\Omega < 200$ the results of both are almost equal if one uses parameters that are scaled by the respective critical values.

Figure 4 visualizes the influence of the Deborah number on the stability of the conductive state. The tongue structure of the stability boundaries in Figs. 4(a) and 4(b) differs considerably from that of the Newtonian fluid (dotted lines). Even very small Deborah numbers $\mathrm{De} \simeq 10^{-3}$ have a measurable impact on the results.

For the parameters of Fig. 4(c), the growth of convection without modulation is oscillatory with the Hopf frequency at onset. For these parameters, a small amplitude modulation produces a quasiperiodic response; see the curve labeled Q that emerges at $\Delta = 0$ out of the Hopf bifurcation threshold $r_{\mathrm{osc}} = 0.079$. With increasing modulation amplitude, however, windows open up where the oscillation frequency of convection is harmonic or subharmonic relative to the modulation frequency Ω.

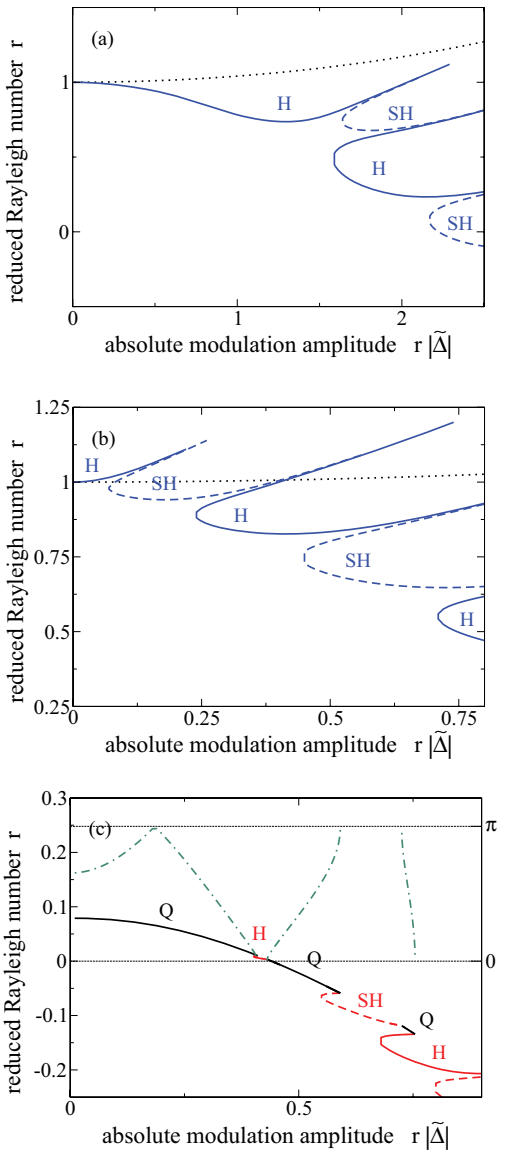

FIG. 4. (Color online) Results of the Floquet stability analysis of the few-modes model for a modulation frequency $\Omega = 13.32$. Bold and dashed lines show the stability boundaries of the modulated conductive state against growth of convection. The bifurcation thresholds for harmonic, subharmonic, and quasiperiodic responses are identified by H, SH, and Q, respectively. The parameters in (a) ($k = 2.22$, $\mathrm{De} = 0.04$) and (b) ($k = 2.22$, $\mathrm{De} = 0.07$) are chosen such that without modulation ($\Delta = 0$) stationary convection grows beyond the stability threshold. The dotted lines show the harmonic bifurcation threshold of a Newtonian fluid ($\mathrm{De} = 0$). For the parameters in (c) ($k = 5.86$, $\mathrm{De} = 0.1$) stationary thermal driving produces oscillatory convection with the Hopf frequency $\omega_H = 57.63$ at onset $r_{\mathrm{osc}} = 0.079$. The Floquet exponent of the quasiharmonic response under modulation is shown by the dash-dotted line. Note the harmonic and subharmonic intervals with exponents 0 and π, respectively.

It is remarkable that the influence of temperature modulation on the stability boundaries of conduction depends so

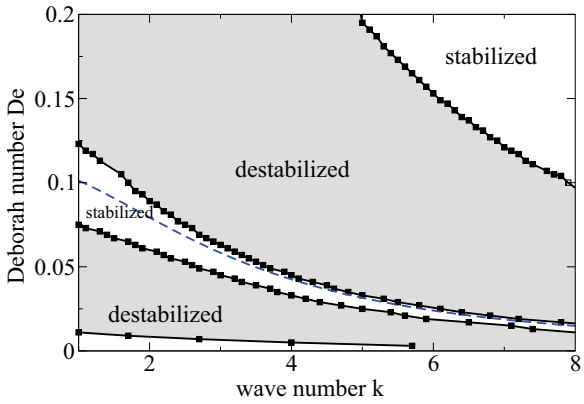

FIG. 5. (Color online) Influence of temperature modulation on the stability behavior of the conductive state for fixed modulation frequency $\Omega = 10$ and amplitude $\Delta = 0.01$ relative to the stability property for $\Delta = 0$. In the regions marked stabilized (destabilized) modulation stabilizes (destabilizes) the quiescent basic state in comparison with the unmodulated case, i.e., the marginal Rayleigh number for $\Delta = 0.01$ is larger (smaller) than the one for $\Delta = 0$. Below the dashed line $\mathrm{De}^*(k, \Delta = 0)$ the instability is stationary without modulation.

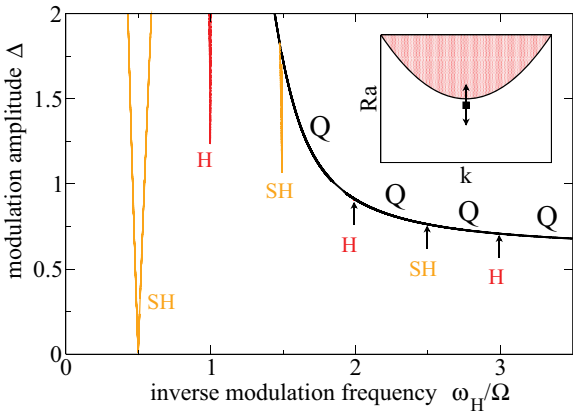

FIG. 6. (Color online) Stability threshold of modulation amplitude Δ versus reduced inverse modulation frequency ω_H/Ω. The bifurcation thresholds for harmonic, subharmonic, and quasiperiodic response are identified by H, SH, and Q, respectively. The mean value $r = r_{\mathrm{osc}}0.99$ of $r(t)$ is fixed to be slightly below the oscillatory threshold r_{osc} under stationary heating ($\Delta = 0$) as shown schematically by the square in the inset. The parabola in the inset refers to the $\Delta = 0$ marginal stability curve and the arrows indicate the action of the modulation. The parameters are $\mathrm{De} = 0.1$ and $k = 6$.

strongly on the parameters. For example, the Deborah numbers in Figs. 4(a) and 4(b) are very similar. Nevertheless, a small amplitude modulation destabilizes the conductive state in (a) but stabilizes it in (b). In order to survey the influence, we determine the stability thresholds for a very small modulation amplitude of $\Delta = 0.01$ and compare them with those of the unmodulated case. The results are shown in Fig. 5 in the k-De plane. In the Newtonian limit $\mathrm{De} \to 0$ one sees the stabilizing effect of modulation that was investigated before [35,38]. Increasing the Deborah number leads in the k-De plane of Fig. 5 to an alternating sequence of parameter regions with destabilization and stabilization. Similar results were also obtained for different values of the modulation amplitude $\Delta = 0.001, \ldots, 0.05$.

We also investigated the stability changes that are induced by modulation of $r(t)$ from a different perspective. In order to do that, we kept the mean Rayleigh number r fixed at a value that is slightly subcritical under stationary heating conditions as indicated schematically by the position of the square in the inset of Fig. 6. Then we modulated the temperature difference with increasing amplitude Δ around this mean value until convection arises. Figure 6 shows the amplitude where under these conditions convection appears, i.e., the stability boundary Δ versus ω_H/Ω for a fixed value of $r = 0.99 r_{\mathrm{osc}}$. For the parameters of Fig. 6 the stability behavior is similar to that of a Mathieu oscillator because the impact of the Newtonian fluid is still noticeable. Centered around $\omega_H/\Omega = 1/2$, there is a sizable frequency interval for subharmonic response. There convection oscillating with the Hopf frequency ω_H can be driven already with a very small modulation amplitude. Further periodic windows with harmonic and subharmonic response, respectively, appear alternatingly at $\omega_H/\Omega = n$ (H) and at $\omega_H/\Omega = n + 1/2$ (SH) with n being integer. Their width decreases with increasing n. Between the above periodic intervals convection grows quasiperiodically as indicated in Fig. 6 by those parts of the stability curve that are labeled by Q and that are connected to the periodic parts.

C. Nonlinear results

We performed extensive numerical calculations to elucidate the nonlinear behavior of convection under modulation. We studied in detail modulated SOC, TW, and SW convection. In the modulated SOC state the rolls remain spatially fixed and only their amplitude oscillate. This type of convection showed the largest response to modulation. For the parameters that we investigated here, the modulated TWs showed practically no oscillations of the phase velocity and only minor amplitude oscillations. Also the SWs that we studied were only slightly amplitude modulated. We also mention that despite an extensive numerical search we did not find TWs that became stabilized by the action of temperature modulation.

So, in the following we only present some results concerning modulated SOC convection that we obtained from finite-difference simulations using the LMF and the UCM field equations. We found that for small modulation frequencies and small Deborah numbers the difference between these two fluid models shows up only via a relatively small difference in the flow amplitudes while the dynamical behavior of the convective response to modulation is the same. This can be seen in detail in Fig. 7. There we show the time variation of the maximum $w_{\mathrm{max}}(t)$ of the vertical velocity field—for better visibility over two modulation cycles. Here w_{max} refers to the maximum over the whole fluid layer.

In Fig. 7 the mean Rayleigh number is well below the marginal stability value $\mathrm{Ra}_{\mathrm{stat}}$ for growth of convection under stationary heating conditions. The time variation of $\mathrm{Ra}(t)$ is shown in Fig. 7(a). As indicated by the shaded areas in Fig. 7(a) it exceeds the stationary threshold $\mathrm{Ra}_{\mathrm{stat}}$ only during the time intervals that are delimited in Fig. 7 by the dotted vertical lines. Note, however, that the modulation amplitude $\Delta = 1$ in

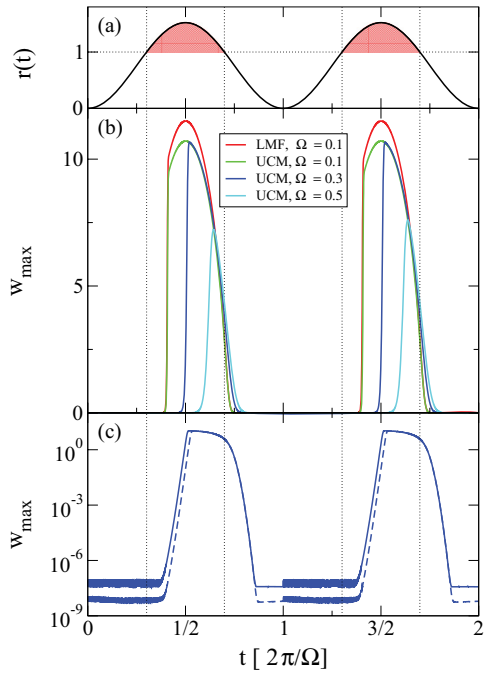

FIG. 7. (Color online) Convective response of a weakly elastic fluid to temperature modulation with large amplitude and small frequencies Ω as indicated. The time variation of the Rayleigh number is shown in (a). The "supercritical" regime in which $\mathrm{Ra}(t)$ exceeds the onset Rayleigh number $\mathrm{Ra}_{\mathrm{stat}}$ for stationary heating is shaded. The maximum $w_{\max}$ of the vertical velocity field over the whole fluid layer as obtained from finite-difference simulations of LMF and UCM field equations is shown in (b). For the dashed curve in (c) we decreased the numerical "noise" level in our UCM simulations by a factor of 10 compared to the full curve in order to elucidate its role for the growth behavior of convection in the "supercritical" driving regime; see the text for further details. The parameters are $\mathrm{De} = 0.01$, $\Delta = 1$, $\langle \mathrm{Ra}(t) \rangle_t = 500$, $k = \pi/\sqrt{2}$, and $\mathrm{Ra}_{\mathrm{stat}} = 27\pi^4/4$.

Fig. 7 is large and that the modulation frequencies are small. Thus, because the modulation period is large compared to the thermal diffusion time, the driving of the system is modulated in a quasistationary manner and, moreover, it spends long times in a driving regime that is supercritical with respect to the stationary case.

Within each modulation cycle convection begins to grow from small velocity levels that have been attained during the previous "subcritical" regime [$\mathrm{Ra}(t) < \mathrm{Ra}_{\mathrm{stat}}$] as soon as the Rayleigh number $\mathrm{Ra}(t)$ crosses the threshold $\mathrm{Ra}_{\mathrm{stat}}$. Then the typical relaxation oscillation behavior follows that has been observed also for low-frequency modulated Newtonian fluids [37]. Comparing the LMF and the UCM dynamics, one sees that response of the UCM is weaker and that it shows a much higher "noise" level of the fields during the "subcritical" regime.

The noise level in our simulations here is of purely numerical nature. But in experiments it can be expected to be much higher because of internal and external thermal fluctuations and all types of imperfections. This noise acts as perturbations and thus determines the convection level to which the system can drop down during the subcritical regime. And thereby it determines as a kind of initial condition for the growth phase, for example, the time at which convection becomes large enough to be seen in the supercritical regime. To show that, we manipulated the noise level in the UCM field equations in Fig. 7(c). By reducing in the finite-difference simulations the admissible level of the divergence of the velocity field by a factor of 10, the numerical fluctuations decrease, the flow velocity decreases in the subcritical regime, and the growth in the ensuing supercritical regime is delayed (see the dashed line).

V. CONCLUSION

We have investigated the influence of viscoelastic forces on the convection structures that appear close to onset in Maxwellian fluids heated from below. We presented a simple few-modes model. Its predictions concerning stationary and oscillatory structures are in good agreement with results that we obtained by numerical simulations of the full nonlinear field equations for small Deborah numbers. We found stable standing waves for many realistic parameters and a change from forward to backward bifurcation for small wave numbers and small Deborah numbers.

In the presence of a time-periodic temperature modulation, we observed that the linear stability and the linear convective response behavior of the quiescent fluid strongly depend on all system parameters. Furthermore, even the low-frequency-modulated, quasistationary nonlinear structures are sensitive to small changes in the Deborah number. In addition, the differences between the UCM and LMF become visible also for small Deborah numbers when the heating is modulated.

ACKNOWLEDGMENT

We acknowledge support from the Deutsche Forschungsgemeinschaft.

[1] H. Bénard, Rev. Gen. Sci. Pures Appl. **11**, 1261 (1900).
[2] J. W. S. L. Rayleigh, Philos. Mag. **32**, 529 (1916).
[3] E. Bodenschatz, W. Pesch, and G. Ahlers, Annu. Rev. Fluid Mech. **32**, 709 (2000).
[4] L. D. Landau and E. M. Lifshitz, *Fluid Mechanics* (Pergamon Press, Oxford, 1987).
[5] J. K. Platten and J. C. Legros, *Convection in Liquids* (Springer-Verlag, Berlin, 1984).
[6] R. G. Larson, Rheol. Acta **31**, 213 (1992).
[7] C. M. Vest and V. S. Arpaci, J. Fluid Mech. **36**, 613 (1969).
[8] H. Harder, J. Non-Newtonian Fluid Mech. **39**, 67 (1991).
[9] M. Avgousti, B. Liu, and A. N. Beris, Int. J. Numer. Methods Fluids **17**, 49 (1993).
[10] E. N. Lorenz, J. Atmos. Sci. **20**, 130 (1963).
[11] R. E. Khayat, Phys. Rev. E **51**, 380 (1995).
[12] R. E. Khayat, J. Non-Newtonian Fluid Mech. **63**, 153 (1996).

[13] E. Abu-Ramadan, J. M. Hay, and R. E. Khayat, J. Non-Newtonian Fluid Mech. **115**, 79 (2003).
[14] P. G. Siddheshwar, G. N. Sekhar, and G. Jayalatha, J. Non-Newtonian Fluid Mech. **165**, 1412 (2010).
[15] M. Sokolov and R. I. Tanner, Phys. Fluids **15**, 534 (1972).
[16] I. A. Eltayeb, Proc. R. Soc. London, Ser. A **356**, 161 (1977).
[17] J. Martínez-Mardones and C. Pérez-García, J. Phys.: Condens. Matter **2**, 1281 (1990).
[18] S. Rosenblat, J. Non-Newtonian Fluid Mech. **21**, 201 (1986).
[19] H. M. Park and H. S. Lee, J. Non-Newtonian Fluid Mech. **66**, 1 (1996).
[20] H. R. Brand and B. J. A. Zielinska, Phys. Rev. Lett. **57**, 3167 (1986).
[21] B. J. A. Zielinska, D. Mukamel, and V. Steinberg, Phys. Rev. A **33**, 1454 (1986).
[22] J. Martínez-Mardones, R. Tiemann, W. Zeller, and C. Pérez-García, Int. J. Bifurcation Chaos Appl. Sci. Eng. **4**, 1347 (1994).
[23] J. Martínez-Mardones, R. Tiemann, and W. Zeller, Chaos, Solitons Fractals **6**, 341 (1995).
[24] J. Martínez-Mardones, R. Tiemann, D. Walgraef, and W. Zeller, Phys. Rev. E **54**, 1478 (1996).
[25] R. B. Bird, R. C. Armstrong, and O. Hassager, *Dynamics of Polymeric Liquids* (Wiley, New York, 1987), Vol. 1.
[26] P. C. Martin, O. Parodi, and P. S. Pershan, Phys. Rev. A **6**, 2401 (1972).
[27] C. W. Hirt, B. D. Nichols, and N. C. Romero, Los Alamos National Laboratory Technical Report No. LA-5852, (unpublished).
[28] F. H. Harlow and J. E. Welch, Phys. Fluids **8**, 2182 (1965).
[29] M. C. Cross and P. C. Hohenberg, Rev. Mod. Phys. **65**, 851 (1993).
[30] E. Knobloch, Phys. Rev. A **34**, 1538 (1986).
[31] M. I. Gerritsma and T. N. Phillips, Z. Angew. Math. Phys. **88**, 523 (2008).
[32] F. P. T. Baaijens, J. Non-Newt. Fluid Mech. **79**, 361 (1998).
[33] T. N. Phillips and I. M. Soliman, Numer. Methods Partial Differ. Equ. **7**, 9 (1991).
[34] D. G. Thomas, U. A. Al-Mubaiyedh, R. Sureshkumar, and B. Khomami, J. Non-Newtonian Fluid Mech. **138**, 111 (2006).
[35] Guenter Ahlers, P. C. Hohenberg, and M. Lücke, Phys. Rev. A **32**, 3493 (1985).
[36] D. W. Jordan and P. Smith, *Nonlinear Ordinary Differential Equations* (Oxford University Press, London, 1999).
[37] P. Matura and M. Lücke, Phys. Rev. E **80**, 026314 (2009).
[38] Guenter Ahlers, P. C. Hohenberg, and M. Lücke, Phys. Rev. A **32**, 3519 (1985).